Available online at www.sciencedirect.com
SCIENCE DIRECT
Journal of Catalysis 241 (2006) 1–13
JOURNAL OF CATALYSIS
www.elsevier.com/locate/jcat

Development of a molecular kinetic scheme for methane partial oxidation over a Rh/α-Al_2O_3 catalyst

Ivan Tavazzi, Alessandra Beretta *, Gianpiero Groppi, Pio Forzatti

NEMAS – Centro di Eccellenza per l'Ingegneria dei Materiali e delle Superfici Nanostrutturate, Dipartimento di Chimica, Materiali e Ingegneria Chimica "Giulio Natta," Politecnico di Milano, Piazza Leonardo da Vinci 32, 20133 Milano, Italy

Received 4 January 2006; revised 14 March 2006; accepted 22 March 2006

Available online 6 May 2006

Abstract

A kinetic investigation on catalytic partial oxidation of methane over a Rh/α-Al_2O_3 catalyst was addressed using a structured annular reactor specifically designed for studying ultra-fast reactions at high temperatures and very short contact times, out of thermodynamic control. Information on the kinetics of O_2 consumption, so far not available in the literature, were collected with CH_4/O_2/inert-gas tests at varying temperatures, contact times, and diluting gases. By also running $CO/O_2/N_2$ and $H_2/O_2/N_2$ tests, the relative activities of CH_4-, CO-, and H_2-rich combustions were identified. The activation of methane was found to be the rate-determining step of steam reforming based on the results of $CH_4/H_2O/N_2$ tests, in line with recent literature reports. The bulk of the data confirmed that methane partial oxidation proceeds according to an indirect reaction scheme consisting of CH_4 deep oxidation, secondary reactions of CH_4 reforming responsible for syngas formation, the water–gas shift reaction, and consecutive oxidations of H_2 and CO. Molecular kinetic expressions are proposed to explain the wide-ranging experimental campaign.

Keywords: Catalytic partial oxidation; Methane; Rh/α-Al_2O_3; Kinetic investigation; Indirect kinetic scheme; C–H bond activation; Annular reactor

1. Introduction

The catalytic partial oxidation of methane is currently considered a promising nonconventional process for syngas generation. Compared with the existing homogeneous process, the presence of a catalyst allows to considerably shorten the reaction times, decrease the volumes, and lower the operating temperatures, thus enabling the use of air instead of pure O_2 as the oxidant, and inhibiting carbon black formation [1]. The features of reactor simplicity and compactness, together with the rapid response to transient load demands, make this process suitable for stationary and mobile applications related to the development of a medium- to small-scale technology for the production of syngas and H_2 [2]. Such novel applications include small hydrogen production stations for the refueling of H_2-fueled vehicles, small-scale distribution networks, and fuel cells for residential power generation. On-board applications deal with the use of solid oxide fuel cells (SOFCs) for auxiliary power units (APUs) on heavy-duty vehicles to supply power to auxiliary cab devices (e.g., conditioning systems, GPS) and trailers (cryogenic circuits). On-board generation of syngas may also be applied on conventional ICE vehicles to speed up the cold-start phase of catalytic converters and to serve as a reducing gas for NO_x trap regeneration and for the SCR of NO_x. Recently, combustion systems using fuel-rich catalytic combustion before lean-premixed combustion have been tested in advanced-performance gas turbines (ultra-low-emission GTs) [3].

Among several effective catalysts for hydrocarbon partial oxidation [4–7], Rh has been proposed as the best-performing active element and the least-selective catalyst to carbon formation [8,9]. Schmidt and coworkers studied methane partial oxidation over Rh, Pt, and Rh/Pt structured catalysts in adiabatic reactors at contact times as short as 10^{-2}–10^{-4} s [8,10] and observed high selectivity to syngas and product distribution far from the thermodynamic equilibrium, evaluated for the water–gas shift and steam reforming reactions. A direct route to H_2 and CO was invoked. In previous and recent work over Rh-coated supports, these authors reported almost complete conversion of CH_4 with selectivity to H_2 and CO > 90% [11].

* Corresponding author. Fax: +39 02 2399 3318.
E-mail address: alessandra.beretta@polimi.it (A. Beretta).

0021-9517/$ – see front matter
doi:10.1016/j.jcat.2006.03.018

The operating conditions used by Schmidt and coworkers were extremely severe with respect to both the temperature and reactant concentrations, which complicates the discrimination of the role of thermodynamics, of heterogeneous and homogeneous reactions, and of transport phenomena. Chang and Heinemann [12] threw light on these aspects by demonstrating that previous results obtained over Co/MgO by Choudary and coworkers [13–16], who observed a selectivity to syngas higher than the equilibrium value at short contact times and suggested the direct formation of H_2 and CO from methane, were biased by incorrect measurements of the actual catalyst surface temperature. Verykios and coworkers investigated the reaction mechanism under more favorable conditions, at high dilution of the gas mixture and of the catalyst [17], over VIII group noble metals supported on Al_2O_3, SiO_2, and TiO_2, and proposed the indirect production of syngas [18]. Baerns and coworkers adopted a pulse-feed technique to minimize the hot-spot temperature on the catalyst [19–21]. They compared the performance of metallic Rh and Rh/Al_2O_3 and proposed a redox mechanism in which the initial step of methane dissociation is catalyzed by partially oxidized Rh sites, stabilized on the supported system, and disfavored by Rh_2O_3 species, predominant on the unsupported catalyst. Similar conclusions were derived by Marin and coworkers [22,23], who reported that the product distribution is determined by the ratio of oxidized Rh (Rh_2O_3) to metallic Rh and proposed a mechanism in which H_2 and CO are formed as primary products. Deutschmann and coworkers [24] proposed a combination of both direct and indirect pathways and gave a detailed surface reaction mechanism consisting of 38 reactions among 6 gas-phase species and 11 surface species. Similar models including only elementary reactions characterized by surface science techniques have been proposed by Froment et al. [25] and Schmidt et al. [26]. On the basis of a microkinetic C_1 model developed by adopting a hierarchical multiscale methodology, Mhadeshwar and Vlachos [27] suggested that H_2 is produced via steam reforming, whereas CO is directly formed by partial oxidation of CH_4. Iglesia and coworkers corroborated the importance of eliminating diffusive limitations and accounting for thermodynamics to properly study the kinetics of methane activation over several catalysts [28,29].

The development of reaction kinetics is a crucial issue in reactor design and optimization by mathematical models. Notwithstanding several previous investigation, there is a general lack of kinetic schemes validated in an operating range relevant to practical applications. In this work, catalytic tests were run under operating conditions suitable to obtain kinetically informative data, wherein the chemical effects can be decoupled from thermodynamic and transfer phenomena effects. Experiments were performed in a structured annular reactor specifically designed to investigate the kinetics of very fast reactions [30], which allows to control the extent of mass transfer limitations, to analyze the process far from the thermodynamic equilibrium and to realize well-controlled temperature conditions with minimum axial gradients.

The data reported herein extend the findings of previous studies [31,32] on the effects of temperature and gas hourly space velocity (GHSV) that were quantitatively explained by an indirect kinetic scheme wherein the complexity of the reacting system [24–29] was reduced to few main molecular stoichiometries. The scheme includes an initial step of complete methane combustion, followed by secondary reactions of methane steam and CO_2 reforming, responsible for syngas production, accompanied by the water–gas shift reaction and consecutive oxidations of CO and H_2. In this study, effort was focused on defining the main kinetic dependencies that affect the single reactions; toward this purpose, the main reactions were isolated and studied separately.

2. Experimental

2.1. Catalyst

The kinetic study was carried out over a 0.5% (wt/wt) Rh/α-Al_2O_3 catalyst, prepared by grafting alumina powders with $Rh_4(CO)_{12}$. A detailed description of the preparation procedure and the characterization of the catalytic system has been given previously [33–37]. Measurements of metal dispersion carried out on fresh samples by H_2 pulse chemisorption showed a Rh dispersion of about 70%.

2.2. Annular reactor

Catalytic tests were performed in an annular duct reactor [38,39] in which a catalytic layer (40–50 μm thick) is deposited according to an optimized procedure [40] over a mullite tube that is coaxially inserted into an outer quartz tube, giving rise to an annular duct through which the gas mixtures flow in laminar regime (Fig. 1). Catalyst loadings were on the order of 10 mg. The mullite support also served as a well for a sliding K-type thermocouple by which the axial profiles of the catalyst temperature were measured. The correspondence of the measurements to the actual temperatures on the catalyst surface was ensured by the thermal equilibrium across the section of the ceramic tube, due to the negligible contribution of the thermal dispersion along the mullite tube on the overall heat dissipation [41]. The average catalyst temperature was calculated as an arithmetic average,

$$\overline{T} = \frac{\sum T_i \Delta x_i}{L},$$

where T_i are the temperatures measured along the axial coordinate of the catalytic layer every 2 mm. The reactor was positioned inside a three-zone tube furnace (Carbolite) equipped with an inner ceramic wall, heated by thermoelectric resistances. Oven temperatures were recorded with a second K-type thermocouple sliding inside a mullite tube located along the heating wall. The effective dissipation of the reaction heat by radiation helped realize catalytic tests at the expense of acceptable thermal axial gradients (mostly below 5 K/cm) compared with those obtained in packed-bed reactors.

In experiments with H_2O cofeed, water was produced in situ by reacting stoichiometric amounts of H_2 and O_2 (added to the reactant mixtures) on a Pt layer deposited upstream from the

Rh coating. The Pt layer was placed outside the heated zone of the furnace and exposed to room temperature, to prevent methane activation. The efficiency of Pt in H_2 burning was tested by delivering the feed mixtures to the reactor heated at low temperature (373 K), to ensure negligible activity of Rh while preventing the condensation of water. At the flow rate used in the partial oxidation and reforming experiments, H_2 conversion was almost complete, and no other reactions were observed. The residual H_2 downstream from the Pt layer was $<0.1\%$ (v/v), and its effect on the catalytic performance of Rh at higher temperatures could be neglected given its extremely high combustion rate over hot Rh surfaces by which H_2 (together with the stoichiometric residual O_2) was completely depleted at the very beginning of the catalytic layer.

2.3. One-dimensional mathematical model of the annular reactor

The annular reactor was modeled according to a one-dimensional heterogeneous isothermal model whose governing equations, written in dimensionless form, are given in Table 1. Gas-phase mass balances along the axial coordinate [Eq. (1)], are coupled with equations of continuity between the catalyst wall and bulk [Eq. (2)] in which the radial mass flow of each species is equal to its overall formation rate. Due to high axial Péclet numbers, axial dispersion was neglected. Resistance to interphase mass transport was described according to a correlation for the Sherwood number [Eq. (3)], derived from the literature and analogous to the Graetz–Nusselt problem of heat exchange in annular ducts with boundary conditions of the third type [39,42–45]. Molecular diffusivity was approximated as binary diffusivity of the ith species in N_2 and calculated according to the Füller–Schettler–Giddings correlation [46]. O_2 intraparticle mass transfer limitations were accounted for by multiplying the rate of the oxidation reactions by a generalized internal effectiveness factor [Eq. (4)], calculated on the basis of the overall O_2 consumption rate [47]. The effective diffusivity of O_2 was calculated according to the Wakao–Smith model (5) assuming an average pore diameter of 100 nm (monomodal pore distribution) and a macropore void fraction (ε_M) of 0.6, determined on the basis of Hg porosimetry measurements.

2.4. Operating conditions

Experiments were run at atmospheric pressure at a temperature of 623–1193 K and a GHSV of $2.0 \cdot 10^6$–$1.1 \cdot$

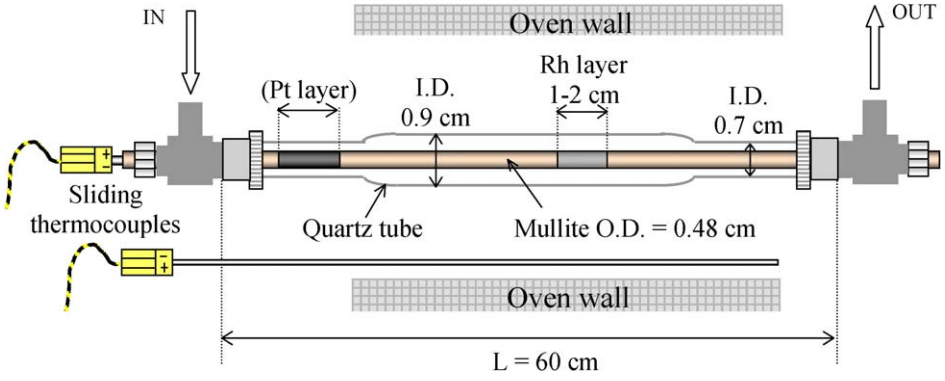

Fig. 1. Sketch of the annular reactor.

Table 1
Sketch of the annular duct and governing equations in the 1D model of the reactor

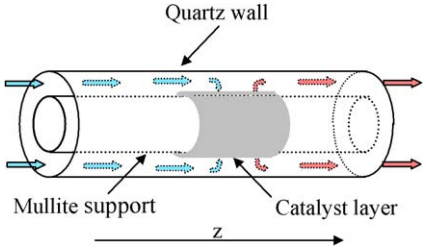

$$\mathrm{Pe}_{\mathrm{m},i} \cdot \frac{\mathrm{d}F_i^*}{\mathrm{d}z^*} = -\frac{4}{1+1/R^*} \cdot \mathrm{Sh}_{\mathrm{loc}_i} \cdot \left(x_i^{\mathrm{b}} - x_i^{\mathrm{w}}\right) \cdot \frac{F_{\mathrm{TOT}}}{F_{\mathrm{TOT}}^{\circ}} \tag{1}$$

$$\mathrm{Sh}_{\mathrm{loc}_i} \cdot \left(x_i^{\mathrm{b}} - x_i^{\mathrm{w}}\right) = \sum_j \nu_{i,j} \cdot \alpha_i \cdot r_j \tag{2}$$

$$\mathrm{Sh}_{\mathrm{loc}_i} = \mathrm{Sh}_{\mathrm{inf}} + 6.874 \cdot e^{(-71.2 z_{\mathrm{Sh},i})} \cdot (1000 \cdot z_{\mathrm{Sh},i})^{-0.35} \tag{3}$$

Generalized internal efficiency

$$\eta_{\mathrm{O_2}}^{\infty} = \frac{\sqrt{2}}{\delta_{\mathrm{L}} \cdot r_v(C_{\mathrm{O_2}}^{\mathrm{S}})} \cdot \left[\int_0^{C_{\mathrm{O_2}}^{\mathrm{S}}} D_{\mathrm{eff,O_2}} \cdot r_v(c) \cdot \mathrm{d}c\right]^{1/2}$$

$$\phi_{\mathrm{O_2}} = \frac{1}{\eta_{\mathrm{O_2}}^{\infty}} \qquad \eta_{\mathrm{O_2}} = \frac{\tanh(\phi_{\mathrm{O_2}})}{\phi_{\mathrm{O_2}}} \tag{4}$$

D_{eff}: random pore model (Wakao–Smith)

$$D_{\mathrm{eff,O_2}} = \varepsilon_{\mathrm{M}}^2 \cdot D_{\mathrm{M}} + \frac{\varepsilon_{\mu}^2 \cdot (1 + 3 \cdot \varepsilon_{\mathrm{M}})}{1 - \varepsilon_{\mathrm{M}}} \cdot D_{\mu} \tag{5}$$

10^7 NL kg_{cat}^{-1} h^{-1}. Calibrated gas mixtures were obtained using mass flow controllers and delivered to the reactor through stainless steel lines. Reactants were highly diluted (inert gas >90%) to reduce the axial temperature gradients along the catalytic layer. The composition of feed and product mixtures was measured by gas chromatography. N_2, O_2, CH_4, CO, H_2O, and CO_2 were analyzed in a VARIAN 3400 (Varian Instrument Group) equipped with a thermal conductivity detector (TCD), a molecular sieve (5 Å) column, and a Porapak QS column with He as carrier gas. H_2 concentration was measured using Ar as carrier gas in a MEGA 5340C (Carlo Erba Strumentazione) equipped with a molecular sieve (5 Å) column and a TCD. N_2 was used as an internal standard for quantifying the net molar flows. At a given feed composition and flow rate, the reaction temperature was progressively increased stepwise, and product analyses were recorded under steady-state conditions, 20 min after each new set point temperature was reached. Blank runs, performed preliminarily over the whole temperature range with no catalyst deposited on the mullite tube, indicated the chemical inertness of the ceramic support and the absence of homogeneous reactions below 1173 K. In all experiments, mass balances of converted C, H, and O were closed between 0.95 and 1.05.

3. Results

3.1. $CH_4 + O_2$ tests: experimental effect of temperature and contact time

A previous study [32] reported the results of CH_4/O_2 tests in an annular reactor in terms of the effects of temperature and GHSV. Those data suggested the formulation of an indirect kinetic scheme. For the sake of clarity, we summarize those previous conclusions herein by discussing independent experiments in which the combined effect of temperature and contact time on the same reaction system was investigated; results are reported in Fig. 2. At each GHSV, deep oxidation of CH_4 occurred in the low-temperature range (roughly between 673 and 843 K), with H_2O and CO_2 the only species produced; reactant conversion increased moderately with temperature. A significant increase in conversion occurred with further increases in temperature. O_2 consumption was eventually limited by mass transfer, reaching an asymptotic value that decreased with increasing GHSV. A significant net production of H_2 and CO started above the temperature (depending on the GHSV) at which O_2 entered diffusive limitation and in-

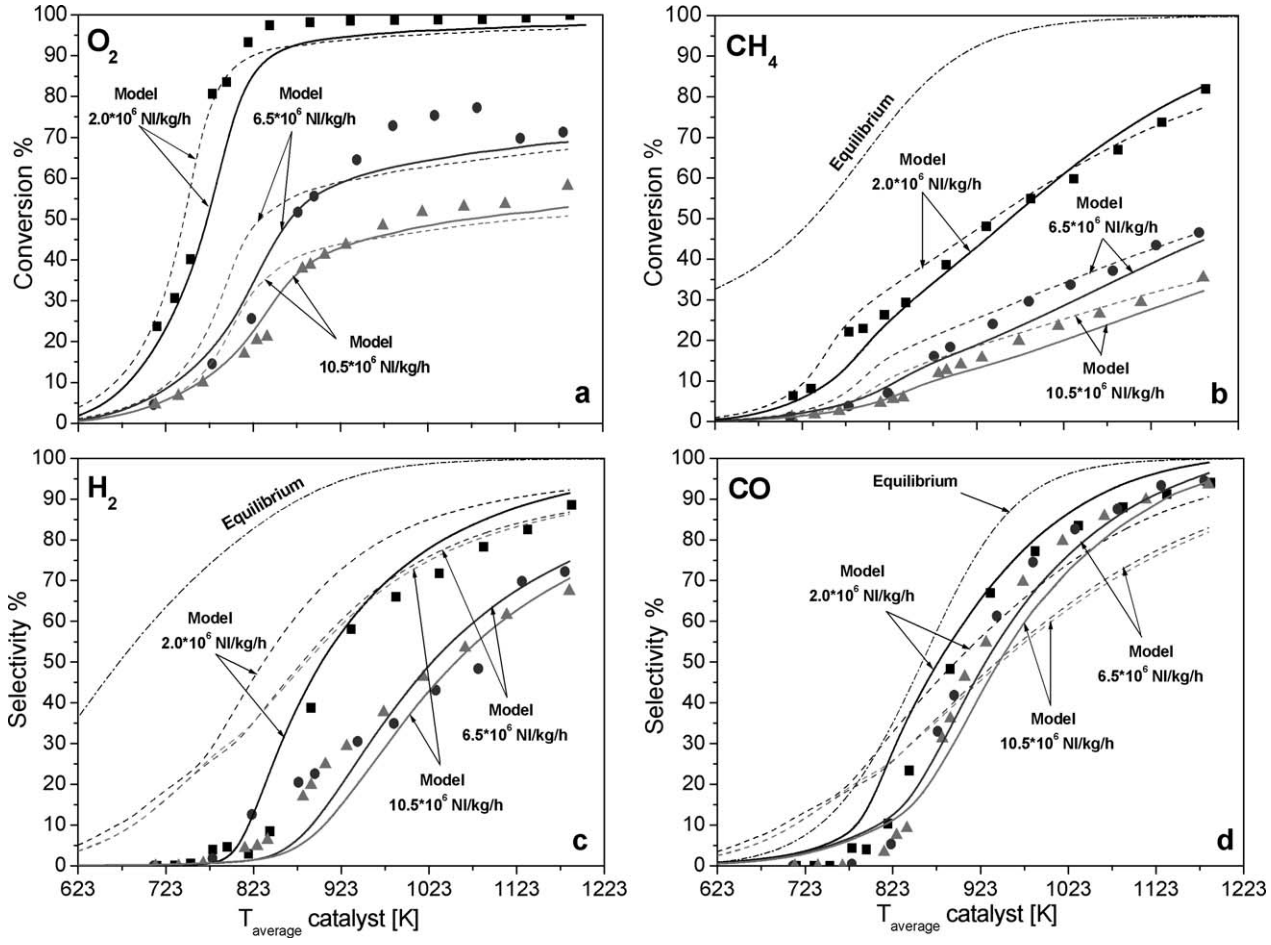

Fig. 2. Combined effect of temperature and GHSV on experimental (symbols) and calculated (lines) reactants conversion (a, b) and syngas selectivity (c, d) in experiments with the reacting system $CH_4 + O_2$: (■) GHSV $= 2.0 \cdot 10^6$ NL kg_{cat}^{-1} h^{-1}, (●) GHSV $= 6.5 \cdot 10^6$ NL kg_{cat}^{-1} h^{-1}, (▲) GHSV $= 10.5 \cdot 10^6$ NL kg_{cat}^{-1} h^{-1}; (- - -) model without consecutive oxidations of CO and H_2, (—) model with consecutive oxidations. Feed composition: $CH_4/O_2/N_2 = 4/2/94\%$ v/v; atmospheric pressure.

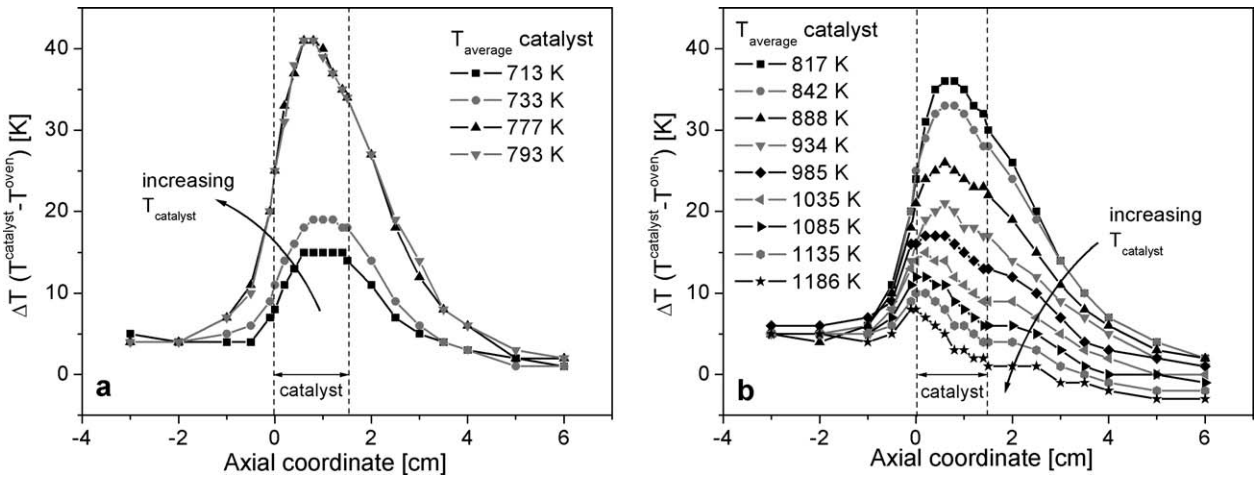

Fig. 3. Axial net temperature profiles obtained by difference between the temperature inside the mullite tube and the temperature in the oven chamber. (a) Sharpening of temperature profiles with increasing average catalyst temperature in the low temperature field (only H_2O and CO_2 produced); (b) progressive smoothening of temperature profiles at high temperature (O_2 conversion diffusion limited, increasing production of H_2 and CO). Feed composition: $CH_4/O_2/N_2 = 4/2/94\%$ v/v; GHSV $= 2.0 \cdot 10^6$ NL kg_{cat}^{-1} h^{-1}; atmospheric pressure.

creased with temperature along with CH_4 conversion, whereas CO_2 and H_2O were progressively consumed (as shown in Fig. 2 by the monotonically increasing selectivity of synthesis gas). The steep rise in reactant conversion at low temperature was accompanied by a significant heat release that produced relatively pronounced peaks in the axial temperature profiles (Fig. 3). The increasing formation of partial oxidation species at the expense of CO_2 and H_2O and the enhanced efficiency of heat dissipation by radiation at higher temperatures resulted in increasingly smooth temperature profiles. Notably, a maximum was always present at the beginning of the catalyst, followed by a progressive decrease in temperature along the layer, consistent with the occurrence of an exothermic–endothermic reaction sequence. An inspection of the temperature profiles also reveals that along 90% of the catalytic layer, the temperature increases were mostly <5 K and never exceeded 10 K, which, considering the wide range of temperatures investigated, can be considered isothermal conditions suitable for kinetic analysis. Notably, in previous partial oxidation experiments [31] performed in an optimized packed-bed reactor with a catalyst dilution of 1:5, axial temperature gradients rose up to 80 K at the same reactant composition and a GHSV of $5 \cdot 10^5$ NL kg_{cat}^{-1} h^{-1}.

Fig. 2 reports simulations according to a purely combustion-reforming water–gas shift scheme (dashed lines), wherein secondary reactions (steam-reforming, CO_2-reforming, and water–gas shift) were described with rate equations and kinetic parameters derived from a previous study in a packed-bed reactor [31], with the kinetics of methane combustion also deduced from a previous study [32]. This model satisfactorily predicted the trends of reactant conversion but could not correctly describe the distribution of products. Experimentally, the selectivity to H_2 decreased markedly at increasing GHSV while the selectivity to CO remained almost unchanged, especially at high temperature; this resulted in H_2/CO ratios well below 2 at low temperatures and high GHSVs, suggesting that the formation of CO and H_2 was partly independent and not fully constrained by the stoichiometry of the reforming reactions alone. In contrast, the simulations systematically overestimated H_2 selectivity and predicted a stronger dependence of CO selectivity on contact time than was observed in the experiments. To decouple the net production of the two species, consecutive oxidations of H_2 and CO to H_2O and CO_2 were included in the scheme [32]. For the same purpose, alternative reaction paths, as proposed by Mhadeshwar and Vlachos [27], could have been used that consider the oxidation of CH_4 with direct formation of CO and H_2O. Nonetheless, the choice of adopting the stoichiometries of H_2 and CO postcombustion allowed independent study of the reactions taken into account in the scheme. Simulations according to such an indirect-consecutive scheme, with rate equations and kinetic parameters derived in the present work and discussed in detail below, are reported in Fig. 2 as solid lines.

3.2. CO- and H_2-rich combustion tests

Experiments of CO and H_2 combustion were performed under rich conditions ($CO/O_2/N_2$ and $H_2/O_2/N_2$ =4/1/95% v/v) with the intent of reproducing the same conditions that occur during methane partial oxidation. Tests were carried out at 373–973 K at GHSVs of $2.0 \cdot 10^6$, $4.0 \cdot 10^6$, and $8.0 \cdot 10^6$ NL kg_{cat}^{-1} h^{-1}.

CO-rich combustion started at about 503 K independent of the contact time, whose reduction instead entailed a decrease in reactant conversion (Fig. 4a). Considering the run at a GHSV of $2.0 \cdot 10^6$ NL kg_{cat}^{-1} h^{-1}, representative of the general trend of experiments, reactant consumption gradually increased with increasing temperature up to about 603 K. Above this temperature, the slope of the conversion curve decreased moderately, possibly due to the onset of internal mass transfer limitations; yet above 683 K, the dependence of CO consumption on temperature increased again. Inspection of temperature profiles (Fig. 4b) shows the progressive growth of a hot spot with increasing average catalyst temperature, roughly up to 603 K; at higher reaction temperatures, axial profiles progressively smoothed, and the hot spot moved upstream from the

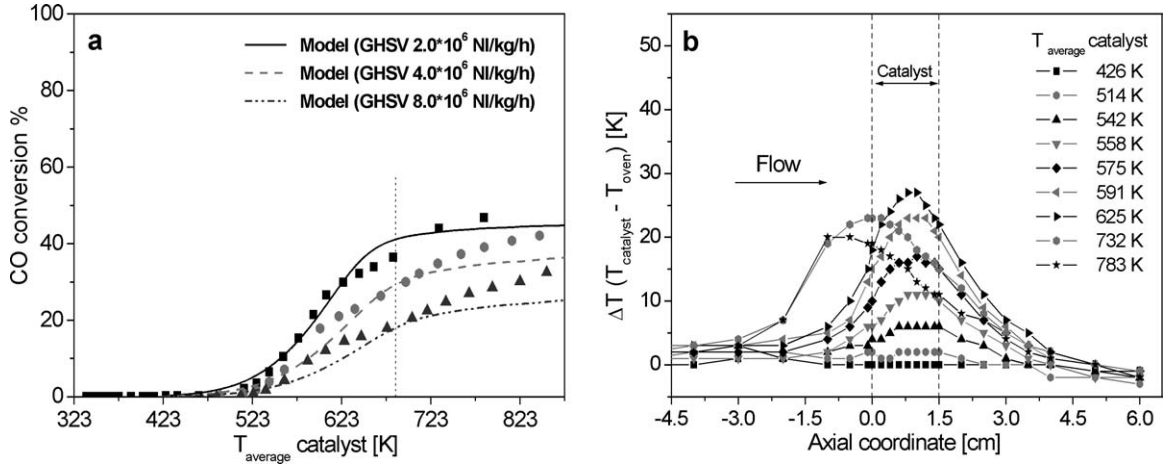

Fig. 4. (a) CO conversion in CO combustion tests under rich conditions at different space velocities. Experimental data: (■) GHSV $= 2.0 \cdot 10^6$ NL $\mathrm{kg_{cat}^{-1}\,h^{-1}}$; (●) GHSV $= 4.0 \cdot 10^6$ NL $\mathrm{kg_{cat}^{-1}\,h^{-1}}$; (▲) GHSV $= 8.0 \cdot 10^6$ NL $\mathrm{kg_{cat}^{-1}\,h^{-1}}$. Model predictions reported as continuous lines. (b) Axial net temperature profiles at GHSV $= 2.0 \cdot 10^6$ NL $\mathrm{kg_{cat}^{-1}\,h^{-1}}$ on increasing catalyst temperature. Feed composition: $CO/O_2/N_2 = 4/1/95\%$ (v/v), atmospheric pressure.

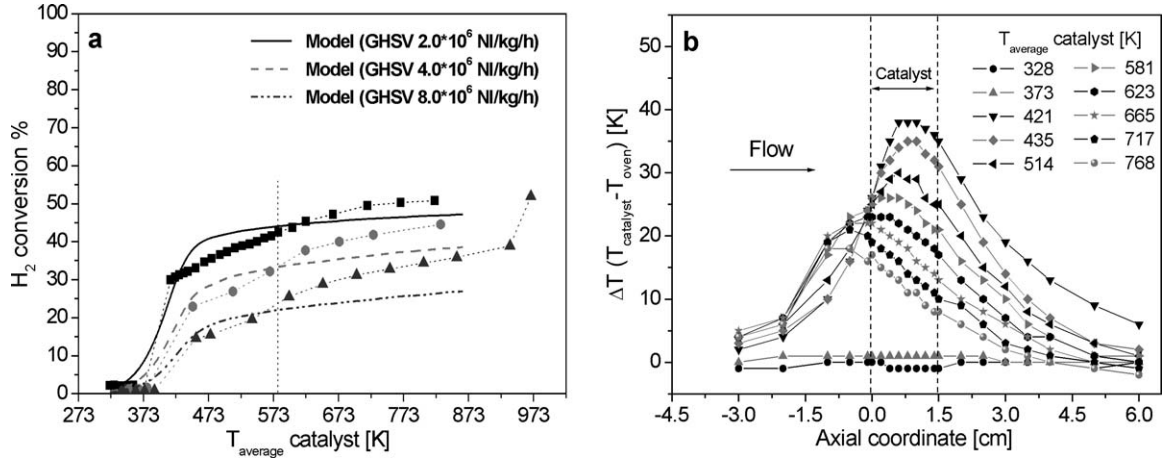

Fig. 5. (a) H_2 conversion in H_2 combustion tests under rich conditions at different space velocities. Experimental data: (■) GHSV $= 2.0 \cdot 10^6$ NL $\mathrm{kg_{cat}^{-1}\,h^{-1}}$; (●) GHSV $= 4.0 \cdot 10^6$ NL $\mathrm{kg_{cat}^{-1}\,h^{-1}}$; (▲) GHSV $= 8.0 \cdot 10^6$ NL $\mathrm{kg_{cat}^{-1}\,h^{-1}}$. Model predictions reported as continuous lines. (b) Axial net temperature profiles at GHSV $= 2.0 \cdot 10^6$ NL $\mathrm{kg_{cat}^{-1}\,h^{-1}}$ on increasing catalyst temperature. Feed composition: $H_2/O_2/N_2 = 4/1/95\%$ (v/v), atmospheric pressure.

catalytic layer, suggesting the onset of gas-phase reactions possibly initiated by the catalyst.

H_2 oxidation under rich conditions started at about 373 K (Fig. 5a), at temperatures more than 100 K lower than those observed in the CO-rich combustion experiments. A stepwise trend was observed; the reaction was in fact so rapid that a diffusive regime was established at low temperatures. At about 573 K, reactant conversion exhibited a moderate step increase, similar to that observed in the CO oxidation tests. Temperature profiles progressively smoothed on increasing H_2 conversion (Fig. 5b) while the hot spot shifted backward and became positioned upstream from the catalyst inlet at temperatures above 603 K, suggesting the presence under these conditions of homogeneous contributions to reactant conversion.

3.3. $CH_4 + O_2 + H_2O$ and $CH_4 + O_2 + CO_2$ tests

The experimental campaign was extended with the aim of better defining the kinetic dependencies of the main reactions and thus improving the chemical consistency of the kinetic scheme. Catalytic runs were performed on a second Rh-coated mullite tube with a catalyst layer similar in weight, length, and thickness to that used in the experiments described above.

Preliminarily, experiments of CH_4 partial oxidation were repeated at a GHSV of $2.6 \cdot 10^6$ NL $\mathrm{kg_{cat}^{-1}\,h^{-1}}$ to compare the performance of the two reactors. Data reported in Fig. 6 show that at low temperatures, in a chemical regime, reactant conversion was congruent with measurements in the first reactor at a GHSV of $2.0 \cdot 10^6$ NL $\mathrm{kg_{cat}^{-1}\,h^{-1}}$, indicating the equivalence of the reactors from a kinetic standpoint; in contrast, a more significant impact of diffusive limitations was observed at high temperatures, as evidenced by a significantly lower asymptotic conversion of O_2. The increased mass transfer resistance was interpreted to result from some degree of eccentricity of the annular duct in the second reactor, due to the flexibility of the long, thin mullite tube. In annular ducts, the external diffusion is strongly affected by the eccentricity; with an aspect ratio of 0.53, the asymptotic Sherwood number of 5.724 with no ec-

centricity is reduced to 2.27 with an eccentricity of 0.5 [45]. By assuming an asymptotic Sherwood number ($Sh_\infty = 3.9$) lower than the value assumed for the first reactor, corresponding to a perfect concentric configuration ($Sh_\infty = 5.724$, $R^* = 0.53$), this effect could be parametrically accounted for (Fig. 6, solid lines). Direct evidence of the impact of external diffusion on reactor performance was obtained by changing the dilution gas from N_2 to He (with a feed composition of $CH_4/O_2/N_2/He = 4/2/8/86\%$ v/v), which roughly tripled the molecular diffusivity of each gas species. At low temperatures (up to about 773 K), the reduced resistance to the interphase mass transfer did not cause any change in reactant conversion due to the prevailing chemical regime established at these temperatures (Fig. 6). Conversely, at high temperatures, whereas the amount of O_2 available at the catalytic surface tended to zero, the asymptotic consumption of O_2 was considerably higher in He than in N_2. Even CH_4 conversion at high temperature was moderately affected by the improved mass transfer in He, suggesting a mixed chemical-diffusive regime induced by the high rate of secondary reactions. Simulations matched the experimental trends satisfactorily, considering the degree of simplification of the mono-dimensional assumption in which the complex fluodynamic effect of the eccentricity was incorporated in a single mass-transfer parameter. The adequacy of the model in accounting for such phenomena allowed a kinetic analysis of data properly decoupled from diffusive limitation effects.

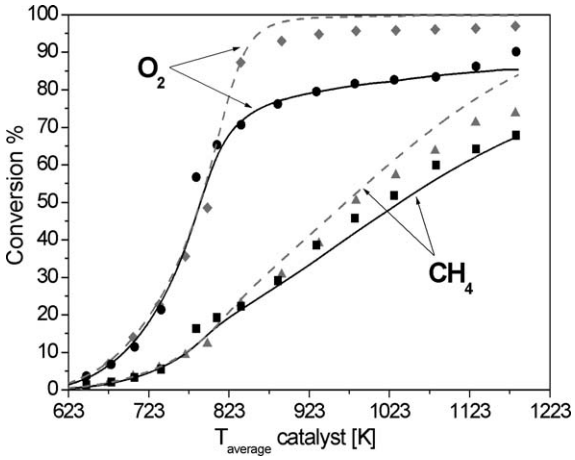

Fig. 6. Effect of external diffusive limitation on reactants conversion in partial oxidation tests. (●) and (■) experimental O_2 and CH_4 conversion in N_2, respectively; (◆) and (▲) O_2 and CH_4 conversion in He. Model predictions: (solid lines) simulation in N_2; (dashed lines) simulation in He. Feed composition: $CH_4/O_2/N_2 = 4/2/94\%$ and $CH_4/O_2/N_2/He = 4/2/7/87\%$ v/v. GHSV $= 2.6 \cdot 10^6$ NL kg_{cat}^{-1} h^{-1}; atmospheric pressure.

The effect of H_2O and CO_2 cofeed on the $CH_4 + O_2$ reaction system was investigated by enriching the gas mixture with 2 and 4% of H_2O and with 2 and 4% of CO_2, respectively. Enrichment with H_2O (Fig. 7) depressed the oxidation of CH_4 at temperatures below 773 K, as evidenced by the significant loss of oxygen conversion at low temperature. The inhibiting effect was remarkable at 2% added water and increased only slightly from doubling the amount of H_2O. Above 823 K, O_2 conversion was independent of the water content in the feed stream, with oxygen consumption under diffusive control. At low temperatures, along with O_2 conversion, CH_4 conversion also decreased on the addition of H_2O to the reactant mixture. With increasing temperature, methane consumption (being under partial kinetic control over the entire temperature range, as discussed above) did not vary, suggesting the independence of secondary reactions on the partial pressure of H_2O.

Fig. 8 reports the trend of oxygen and methane conversion on enriching the feed stream with CO_2. In the case of carbon dioxide addition, data were collected only at 733 and 1033 K (i.e., at temperatures representative of the low- and high-temperature fields), to avoid prolonged exposure of the catalyst to CH_4- and CO_2-rich mixtures, which in previous experiments of methane dry reforming caused deactivation, possibly due to the formation of surface carbonaceous deposits. At inhibiting effect was not observed at either low or high temperatures, indicating the independence of both CH_4 combustion and reforming reactions on CO_2 concentration.

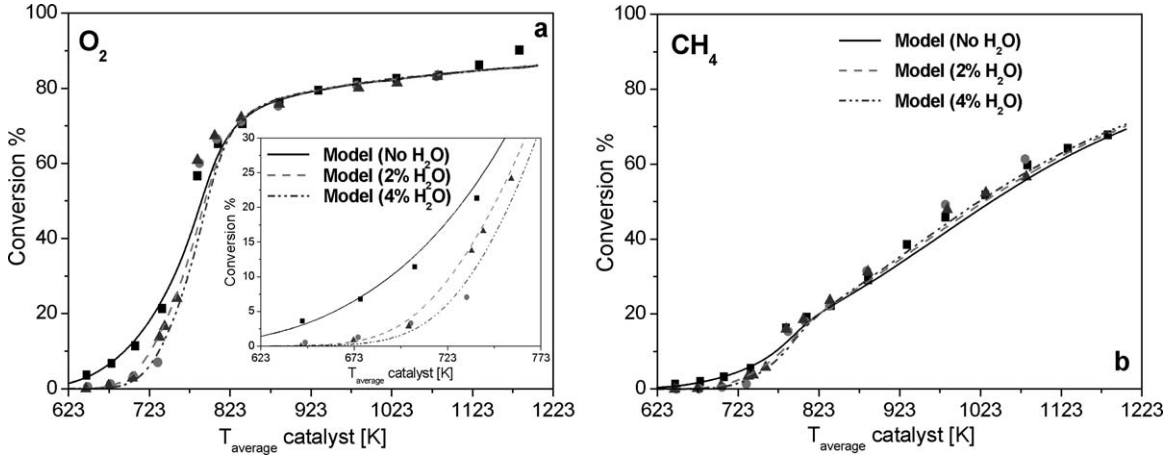

Fig. 7. Effect of H_2O enrichment to the $CH_4 + O_2$ reacting system on O_2 (a) and CH_4 (b) conversion. Experimental results: (■) feed: $CH_4/O_2/N_2 = 4/2/94\%$ (v/v); (●) feed: $CH_4/O_2/H_2O/N_2 = 4/2/2/92\%$ (v/v); (▲) feed: $CH_4/O_2/H_2O/N_2 = 4/2/4/90\%$ (v/v). Model predictions reported as continuous lines. GHSV $= 2.6 \cdot 10^6$ NL kg_{cat}^{-1} h^{-1}, atmospheric pressure.

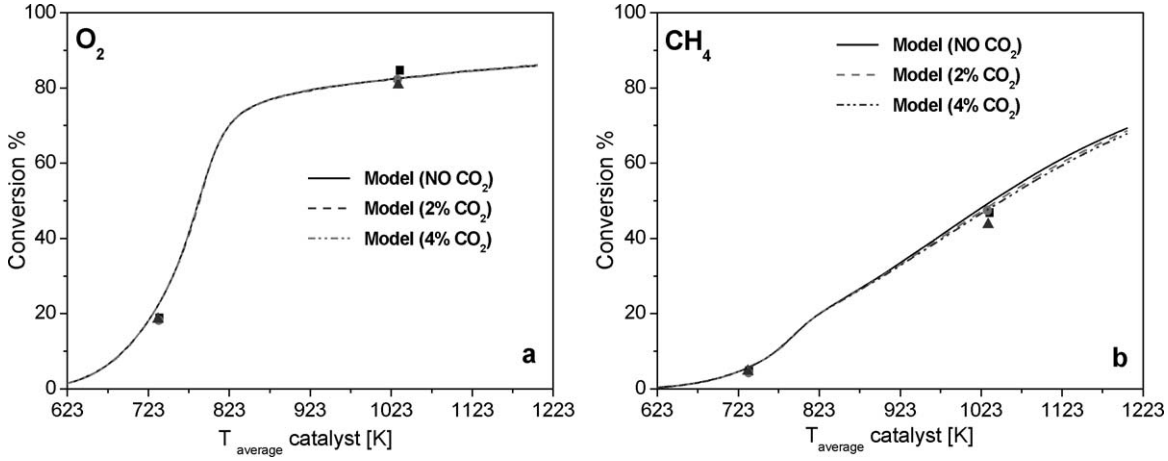

Fig. 8. Effect of CO_2 enrichment to the $CH_4 + O_2$ reacting system on O_2 (a) and CH_4 (b) conversion. Experimental results: (■) feed: $CH_4/O_2/N_2 = 4/2/94\%$ (v/v); (●) feed: $CH_4/O_2/CO_2/N_2 = 4/2/2/92\%$ (v/v); (▲) feed: $CH_4/O_2/CO_2/N_2 = 4/2/4/90\%$ (v/v). Model predictions reported as continuous lines. GHSV $= 2.6 \cdot 10^6$ NL kg_{cat}^{-1} h^{-1}, atmospheric pressure.

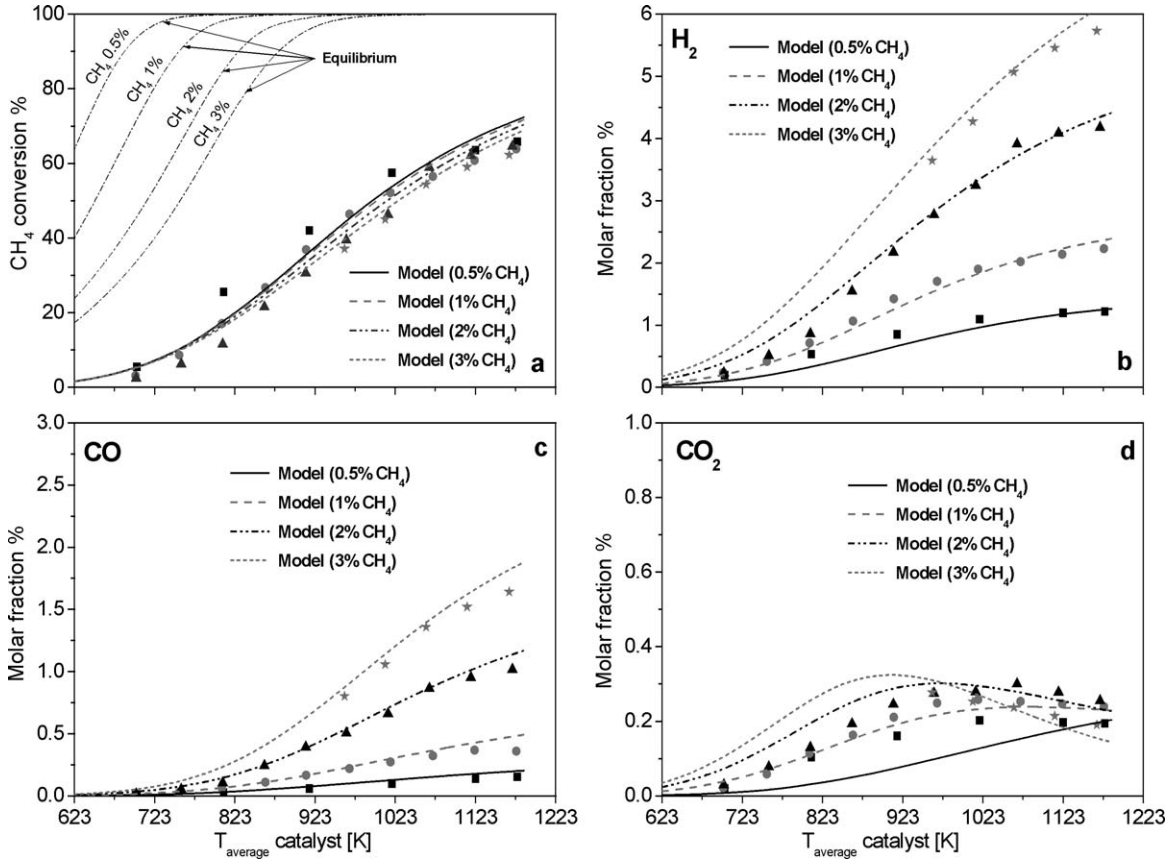

Fig. 9. Effect of CH_4 partial pressure in steam reforming tests (reacting system $CH_4 + H_2O$) on (a) CH_4 conversion and (b, c, d,) products molar fraction. Experimental data: (■) feed: $CH_4/H_2O/N_2 = 0.5/4/95.5\%$ (v/v); (●) feed: $CH_4/H_2O/N_2 = 1/4/95\%$ (v/v); (▲) feed: $CH_4/H_2O/N_2 = 2/4/94\%$ (v/v); (★) feed: $CH_4/H_2O/N_2 = 3/4/93\%$ (v/v). Model predictions reported as continuous lines. GHSV $= 2.6 \cdot 10^6$ NL kg_{cat}^{-1} h^{-1}, atmospheric pressure.

3.4. $CH_4 + H_2O$ tests

The reactivity of the $CH_4 + H_2O$ system was studied by fixing the concentration of one species and changing the amount of the other to investigate the kinetic dependence on the reactant partial pressure. The effect of water was investigated at 2% of CH_4 and at 4, 6, and 8% (v/v) of H_2O; the effect of CH_4 was analyzed at 4% of H_2O and 0.5, 1, 2, and 3% of methane. Mixtures with a H_2O/CH_4 ratio >1 (the stoichiometric ratio for steam reforming) were fed to depress coke formation. For the same reason, the experiment with the lowest H_2O/CH_4 ratio (4/3) was carried out at temperatures above 973 K, because carbon formation is favored at lower temperatures.

Fig. 9 shows the results of steam-reforming tests at various partial pressures of methane. The reaction started at about 693 K, and reactant consumption increased progressively with

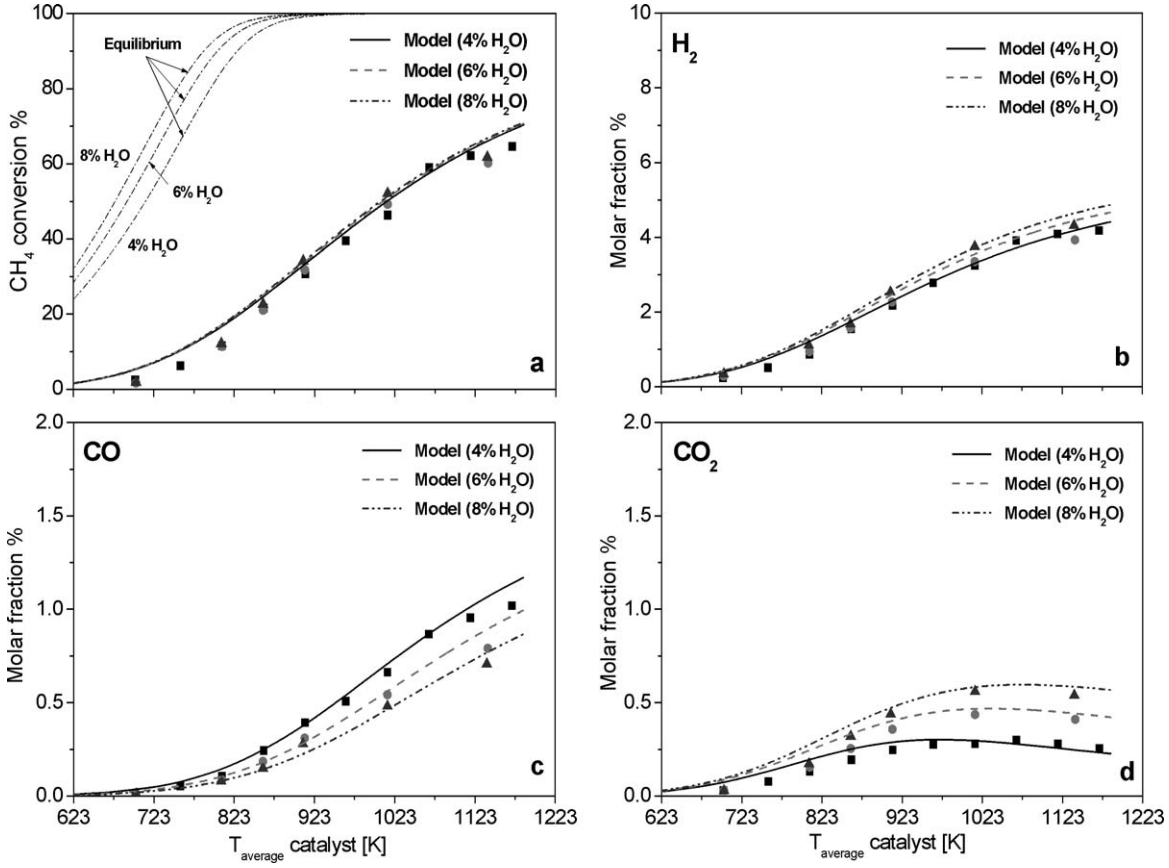

Fig. 10. Effect of H_2O partial pressure in steam reforming tests (reacting system $CH_4 + H_2O$) on (a) CH_4 conversion and (b, c, d,) products molar fraction. Experimental data: (■) feed: $CH_4/H_2O/N_2 = 2/2/96\%$ (v/v); (●) feed: $CH_4/H_2O/N_2 = 2/4/94\%$ (v/v); (▲) feed: $CH_4/H_2O/N_2 = 2/6/92\%$ (v/v). Model predictions reported as continuous lines. GHSV $= 2.6 \cdot 10^6$ NL kg_{cat}^{-1} h^{-1}, atmospheric pressure.

temperature, although remaining significantly lower than the predicted values at thermodynamic equilibrium (dotted lines). H_2 and CO production also increased monotonically with temperature, whereas CO_2 formation passed through a maximum due to the thermodynamics of the water–gas shift reaction, which favors the forward reaction at low temperatures and the reverse reaction at high temperatures. The conversion of CH_4 was weakly dependent on its feed concentration, suggesting that the forward rate of steam reforming was first-order with respect to the partial pressure of methane. The residual moderate dependence, with an increasing trend of conversion at decreasing partial pressure of CH_4, was interpreted as the result of an inhibiting effect due to the competitive adsorption of CO, the concentration of which increased with increasing CH_4 feed content. It is noteworthy that at low temperature, the extent of methane conversion was comparable to that measured in partial oxidation tests, indicating that the rate of intrinsic reforming kinetics in the absence of oxygen was similar to the combustion rate under fuel-rich conditions.

On increasing the inlet partial pressure of H_2O (Fig. 10), methane conversion was totally independent of the excess of water, evidencing a zero-order dependence of the forward reaction rate of steam reforming on H_2O concentration and indicating that thermodynamic constraints played no significant role under the investigated conditions. Concerning the product distribution, the increasing amount of water in the feed mixture promoted the water–gas shift reaction, which progressively shifted the distribution of products toward hydrogen and CO_2.

4. Kinetic analysis

In this work, extending the experimental investigation allowed us to better define the kinetic dependencies of several molecular reactions in the indirect scheme; these are discussed below. The corresponding kinetic parameters, derived by nonlinear regression on experimental data, are reported in Table 2.

4.1. CH_4 combustion

Low-temperature data on the effect of temperature, GHSV, nature of the carrier, and H_2O and CO_2 addition are best described by assuming that the oxidation of methane is proportional to its partial pressure, independent of O_2 concentration and inhibited by H_2O adsorption with kinetics

$$r_{TO} = \frac{k_{TO} \cdot P_{CH_4}}{(1 + K_{H_2O}^{ads} \cdot P_{H_2O})^2}. \quad (6)$$

The lack of an explicit dependence on O_2 is congruent with the picture of high surface coverage from oxygen with few sites available for CH_4 adsorption, in line with findings on Pt and

Table 2
Kinetic equations and parameters obtained in this work

Reaction	Kinetic expression	$k_j^{873\ (K)}$ (mol g^{-1} s^{-1} atm^{-1})	E_{att}/R (K)
Methane combustion $CH_4 + 2O_2 \rightarrow 2H_2O + CO_2$	$R_{CTO} = \frac{k_{CTO} \cdot P_{CH_4}}{(1 + K_{ads,H_2O} \cdot P_{H_2O})^2} \cdot \sigma_{O_2}$	$8.061 \cdot 10^{-3}$	6795
Steam reforming $CH_4 + H_2O \rightarrow 3H_2 + CO$	$R_{SR} = \frac{k_{SR} \cdot P_{CH_4} \cdot (1 - \eta_{SR})}{(1 + K_{ads,O_2} \cdot P_{O_2} + K_{ads,CO} \cdot P_{CO})^2} \cdot \sigma_{H_2O}$	$6.2 \cdot 10^{-3}$	7069
CO_2-reforming $CH_4 + CO_2 \rightarrow 2H_2 + 2CO$	$R_{DR} = \frac{k_{DR} \cdot P_{CH_4} \cdot (1 - \eta_{DR})}{(1 + K_{ads,O_2} \cdot P_{O_2} + K_{ads,CO} \cdot P_{CO})^2} \cdot \sigma_{CO_2}$	$6.2 \cdot 10^{-3}$	7069
Reverse water–gas shift $CO_2 + H_2 \rightarrow CO + H_2O$	$R_{RWGS} = \frac{k_{RWGS} \cdot P_{CO_2} \cdot P_{H_2} \cdot (1 - \eta_{RWGS})}{(1 + K_{ads,O_2} \cdot P_{O_2} + K_{ads,CO} \cdot P_{CO})^2}$	$6.07 \cdot 10^{-1}$ (mol g^{-1} s^{-1} atm^{-2})	3910
CO oxidation $CO + (1/2)O_2 \rightarrow CO_2$	$R_{Ox,CO} = k_{Ox,CO} \cdot P_{CO} \cdot \sigma_{O_2}$	$2.54 \cdot 10^{-1}$	7000
H_2 oxidation $H_2 + (1/2)O_2 \rightarrow H_2O$	$R_{Ox,H_2} = k_{Ox,H_2} \cdot P_{H_2} \cdot \sigma_{O_2}$	4.196	5000

Surface adsorption	$K_{ads,j}^{873\ (K)}$ (atm^{-1})	$\Delta H_{ads}/R$ (K)
O_2	42.53	−7000
H_2O	$2.216 \cdot 10^{-1}$	−19900
CO	15	−3120

Pd [48] and recent results on Rh [49]. Note that on the basis of preliminary data, a negative kinetic dependence on O_2 had been initially assumed [32]; however, subsequent experiments [37] clearly indicated that the kinetics of CH_4 activation by O_2 is independent of O_2 partial pressure and has an overall order lower than 1.

On the addition of water to the inlet mixture, the deep oxidation of CH_4 was markedly depressed, indicating competitive adsorption of H_2O on the catalyst surface and decreased availability of O_2-free sites for CH_4 activation. This trend can be accounted for (Fig. 7, solid lines) by assuming in Eq. (6) a negative dependence with respect to H_2O; the exponent of the adsorption term is consistent with a dissociative adsorption of CH_4 involving two catalytic sites. The apparent saturation of the inhibiting effect of water in the series at 0–2–4% is likely correlated with the progressive increase of the temperature range in which the kinetic data were collected at increasing partial pressure of H_2O, that is, to the attenuation of the inhibition at increasing temperature. A rather high value of apparent heat of H_2O adsorption equal to −165 kJ/mol (Table 2) was functional for capturing the observed trends according to the assumed Langmuir–Hinshelwood rate expression.

4.2. Steam and CO_2 reforming of CH_4

For secondary reactions, the approach to equilibrium was accounted for by introducing the $(1 - \eta_j)$ factor, where η_j is the ratio between the experimental reaction quotient ($K_{P,j}$) and the thermodynamic equilibrium constant ($K_{eq,j}$), so as to identify the actual reaction order and temperature dependence of forward reaction rates. Experimental evidence in reforming tests led to the formulation of rate equations for steam and CO_2 reforming proportional to the partial pressure of CH_4 and independent of the partial pressure of H_2O and CO_2. The slightly increasing trend of CH_4 conversion at decreasing inlet concentration of methane (Fig. 9) was accounted for by invoking an inhibiting effect of CO [Eqs. (7) and (8)].

The extent of CH_4 conversion at low temperature in partial oxidation tests indicated that in the presence of O_2 at temperatures below 773 K, the contribution of reforming reactions was negligible, contrary to what was observed at the same temperatures in CH_4/H_2O experiments. The effect of O_2 on the kinetics of steam reforming at low temperatures (a complex effect that may be related to modifications of Rh coordination) could be accounted for (Fig. 2, solid lines) by introducing an inhibition term. Accordingly, the following expression was proposed:

$$r_{SR} = \frac{k_{SR} \cdot P_{CH_4} \cdot (1 - \eta_{SR})}{(1 + K_{O_2}^{ads} \cdot P_{O_2} + K_{CO}^{ads} \cdot P_{CO})^2}. \quad (7)$$

The kinetic dependencies found with respect to reactants partial pressure were in agreement with recent studies of Wei and Iglesia [29], who reported the independence of methane activation rate on the nature and amount of coreactants. They investigated CH_4 reforming over Rh clusters by means of kinetic and isotopic tracer methods and provided a simple and unifying mechanistic proposal for it. They found that activation of the C–H bond was the sole kinetically relevant step, and that turnover rates were dependent only on Rh crystallite size and independent of the nature of the support. Although Wei and Iglesia provided data concerning the negligible role of competitive adsorption on methane activation, in this work surface saturation was taken into account as an important kinetic effect. It should be noted that the present experimental work spanned a very wide temperature window.

Concerning CO_2 reforming, catalyst deactivation phenomena on exposure to CH_4/CO_2-rich mixtures did not allow us to

directly investigate the reaction in the annular reactor. Analysis of data and previous investigations support the kinetic relevance of this consecutive step. In $CH_4/O_2/N_2$ experiments, we systematically observed that at increasing temperature, the H_2/CO ratio tended to increase to an asymptotic value (∼1.7) below the equilibrium value of 2. Such a dependence on temperature could not be accounted for by invoking only the steam-reforming and water–gas shift reactions; an important contribution from CO_2 reforming had to be included to decrease the calculated value of the H_2/CO ratio at high temperature and match the experimental data. Besides, previous studies performed in an optimized packed-bed reactor under kinetically informative conditions [31] indicated the activity of Rh toward CO_2 reforming, with a resulting reaction rate comparable in order of magnitude to the rate of steam reforming (with a ratio $k_{CO_2\text{-R}}/k_{SR}$ equal to about 0.25 at all temperatures). On the basis of these considerations and the mechanistic findings of Wei and Iglesia mentioned above, we assumed for the reaction of CO_2 reforming the same rate equation proposed for the reaction of steam reforming, with $k_{CO_2\text{-R}} = k_{SR}$:

$$r_{CO_2\text{-R}} = \frac{k_{CO_2\text{-R}} \cdot P_{CH_4} \cdot (1 - \eta_{CO_2\text{-R}})}{(1 + K^{ads}_{O_2} \cdot P_{O_2} + K^{ads}_{CO} \cdot P_{CO})^2}. \quad (8)$$

Notably, under conditions of high dilution and low conversion (i.e., at low reaction temperature) the kinetics of CH_4 steam reforming and CH_4-rich combustion tend to reduce to the simple form $r_j = k_j \cdot P_{CH_4}$, in agreement with previously reported results [29]. According to our results, $k_{TO} \sim k_{SR}$, in line with the hypothesis that both oxidation and reforming are kinetically controlled by C–H bond activation. According to our interpretation, the rate-determining step involved in either the combustion or the reforming of CH_4 is independent on the state of the catalyst surface (O_2-covered or clean). In contrast, the prevailing stoichiometry is determined by the surface environment surrounding the adsorbed C^* and H^* intermediates; in this respect, the conversion of CH_4 by steam reforming was depressed when high O_2 surface coverage was present. Referring the values reported in Table 2 to the number of exposed surface Rh atoms measured by H_2 chemisorption (at Rh dispersion of 70%), k_{TO} and k_{SR} at 873 K are equal to 0.24 and 0.18 $s^{-1}\,kPa^{-1}$, respectively. These estimates are very close to the values reported by Wei and Iglesia relative to methane conversion in reforming reactions [29]. Nonetheless, in contrast to the findings of Wei and Iglesia [49], our study evidenced a very similar dependence of the reaction rates of methane combustion and steam reforming on temperature, with activation energies equal to 56 and 59 kJ mol^{-1}, respectively. These values resemble those reported by Liu and Hu for dissociative adsorption of CH_4 on flat Rh(111) surfaces calculated by density functional theory [50]; however, they are significantly lower than those reported by several authors for CO_2 reforming over Rh-supported catalysts, which range from 90 to 100 kJ mol^{-1} [29]. Actually, for CH_4-rich combustion, Wei and Iglesia found an activation energy of 55 kJ mol^{-1} [49], very close to our estimate reported here, but for methane activation in absence of O_2, they derived an activation energy of about 110 kJ mol^{-1}, in agreement with the values reported in the literature [29].

Finally, note that to account for the annihilation of reaction rates in the case that the partial pressure of the coreactant approached zero, which does not appear explicitly in the proposed kinetic equations, the rate expressions of CH_4 combustion, steam reforming and CO_2 reforming were multiplied by σ_{O_2}, σ_{H_2O}, and σ_{CO_2}, respectively, where σ_i is a "limiting" factor defined as

$$\sigma_i = \frac{p_i}{10^{-6} + p_i}. \quad (9)$$

The threshold value (10^{-6} atm) at the denominator, under which the kinetics tend to be first-order with respect to the partial pressure of the coreactant as well, was chosen to be the smallest number that guaranteed numerical convergence in simulations. In this respect, here we did not imply a specific physical meaning. An analysis of sensitivity revealed negligible variations in model predictions up to values of 10^{-4} atm. Of course, kinetic equations that are independent of the partial pressure of the limiting reactant cannot be used in reactor simulations, because they will lead to overconsumption of coreactant, exceeding the limit allowed by molecular stoichiometries at the catalyst wall.

Concerning the water–gas shift reaction, an accurate description of the experimental results (Figs. 9 and 10) was achieved by adopting the following rate equation (written in reverse form):

$$r_{RWGS} = \frac{k_{RWGS} \cdot P_{CO_2} \cdot P_{H_2} \cdot (1 - \eta_{RWGS})}{(1 + K^{ads}_{O_2} \cdot P_{O_2} + K^{ads}_{CO} \cdot P_{CO})^2}, \quad (10)$$

with negative dependence on O_2 and CO partial pressure conserved to ensure congruence with equations of reforming reactions. The sensitivity of the calculated CO_2 molar fraction to the kinetics of the water–gas shift reaction allowed tuning of the corresponding parameters even though the reaction was not independently investigated. Note, however, that above 873 K, the observed kinetics of the water–gas shift were significantly affected by the approach to equilibrium conditions (with η_{WGS} between 0.2 and 0.5), which could have biased estimation of the kinetic parameters.

4.3. CO and H_2 combustion

Kinetic parameters for H_2 and CO oxidation were derived by assuming for these reactions the simplest possible expressions (i.e., first-order with respect to the fuel species), given the lack of direct information on the reaction orders [Eqs. (11) and (12)]. Experiments with H_2/CO/O_2 mixtures under rich conditions gave evidence of the inhibiting effect by CO on the oxidation of H_2; nonetheless, no inhibition contributions were included in the kinetics given the difficulty in extrapolating the adsorption constants to the temperature field of interest for CH_4 partial oxidation:

$$r_{H_2\text{-comb}} = k_{H_2\text{-comb}} \cdot P_{H_2} \quad (11)$$

and

$$r_{CO\text{-comb}} = k_{CO\text{-comb}} \cdot P_{CO}. \quad (12)$$

Both expressions in the model mass balances were multiplied by σ_{O_2}, the coreactant-limiting factor. Fitting to the experimen-

tal data was carried out at 353–523 K for H_2 combustion and at 473–673 K for CO combustion, that is, in temperature windows in which no evidence of homogeneous contributions to the reaction was observed. At increasing temperature, on entering a diffusive regime, radicalic reactions (possibly induced by the presence of the catalyst) occurred because reactant consumptions were higher than the asymptotic values predicted by the model (Figs. 4a and 5a) representing the upper conversion limit for the catalytic reaction. The comparison among the kinetic constants reported in Table 2 at 873 K indicates a scale of rich combustion reactivity, H_2:CO:CH_4, in order of magnitude equal to 700:30:1, in agreement with estimates derived preliminarily by fitting the experimental data for methane partial oxidation [32]. The estimated CO/CH_4 relative oxidation rate closely resembles the reactivity ratio of 40 observed under different conditions in previous work [49].

According to the scenario depicted in the present study, the overall process of methane partial oxidation proceeds through different phases determined by the nature of the species adsorbed on the catalyst surface. In the presence of high O_2 surface coverage, which is thermodynamically favored at low temperatures, only CO_2 and H_2O are produced by deep oxidation of methane; methane reforming is strongly inhibited. The rate of O_2 consumption increases with temperature, causing a reduction in the O_2 surface coverage, which promotes the reactions of reforming. H_2 and CO are formed and converted to H_2O and CO_2 along the entire catalyst length, in turn causing depletion of the surface O_2, which eventually drives O_2 into mass transfer limitations. The cleaning of O_2 from the surface considerably enhances the reforming reaction rates and thus CH_4 consumption. Such a self-promoting mechanism induces a "chemical lightoff" of the process associated with a stepwise cleanup of the catalyst surface from O_2, after which a net production of synthesis gas can be established, in line with findings of Lyubovsky et al. [3]. At the high temperatures representative of practical applications, reforming reactions are active from the very start of the catalyst; O_2 is rapidly depleted by H_2 and CO postcombustion, which is predicted to occur mostly near the entrance of the catalytic layer.

5. Conclusion

The potentialities of the annular reactor were exploited to obtain highly informative kinetic data on extremely fast reactions involved in the partial oxidation of CH_4 over Rh/α-Al_2O_3. The comparison between experimental results and predictions of a mono-dimensional model of the annular reactor corroborated the evolution of the process according to an indirect-consecutive scheme (previously proposed by us) consisting of a primary reaction of CH_4 deep oxidation to CO_2 and H_2O, followed by secondary reactions of steam and CO_2 reforming of CH_4, responsible for syngas production, the water–gas shift reaction, and the consecutive combustion of H_2 and CO. The invariance of reactants conversion at high temperatures in partial oxidation experiments after enriching the feed stream with CO_2 and H_2O was confirmed by the independence of the forward reaction rate of CH_4 reforming on the coreactant partial pressure. This implies that H_2O enrichment doest not exert a kinetic promotional effect on H_2 yield in catalytic partial oxidation over Rh catalyst, but a thermodynamically controlled promotion can be realized at sufficiently low GHSV. Our findings agree with and extend the results reported by Wei and Iglesia concerning the independence of CH_4 activation on the nature and amount of coreactant for single reactions; however, adsorption and inhibition phenomena play significant roles at high conversion values, and the kinetics of steam reforming are markedly inhibited in the presence of O_2. By means of simple kinetics, a fine description of the CPO reacting system was achieved (Fig. 2, solid lines) within a very wide range of operating temperatures (623–1173 K) and GHSVs (10^6–$2.5\cdot10^7$ NL kg_{cat}^{-1} h^{-1}). Molecular equations developed herein are proposed as a kinetic output of practical interest for reactor design and optimization.

Acknowledgments

This work was supported by MIUR-Rome, the EU Cathlean Project, and the Center for Nano-Engineered Materials and Surfaces.

Appendix A. Nomenclature

$x_i^{w(b)}$	wall (bulk) molar fraction
$\mathcal{D}_i$	molecular diffusivity ($m^2\,s^{-1}$)
z	axial coordinate (m)
z^*	dimensionless axial coordinate ($= z/d_h$) (–)
F_i	molar flow of species ith ($mol_i\,s^{-1}$)
F°_{TOT}	total inlet molar flow ($mol\,s^{-1}$)
F_i^*	F_i/F°_{TOT} dimensionless flow of species ith (–)
R^*	R_{int}/R_{out} (aspect ratio) (–)
d_h	hydraulic diameter (m)
$Pe_{m,i}$	Péclet number, $Re\cdot Sc_i$ (–)
v	average gas velocity ($m\,s^{-1}$)
Re	Reynolds number $= vd_h/\nu$ (–)
Sc_i	Schmidt number $= \nu/\mathcal{D}_i$ (–)
$K_{c,i}$	mass transfer coefficient ($m\,s^{-1}$)
Sh_i	local Sherwood number $= K_{c,i}d_h/\mathcal{D}_i$ (–)
$Z_{Sh,i}$	$z^*/Pe_{m,i}$ (–)
r_j	reaction rate ($mol\,s^{-1}\,kg^{-1}$)
$C^S_{O_2}$	O_2 concentration at the catalyst wall ($mol\,m^{-3}$)
D_M	macroporous diffusivity ($m^2\,s^{-1}$)
D_μ	microporous diffusivity ($m^2\,s^{-1}$)

Greek symbols

ν	cinematic viscosity ($m^2\,s^{-1}$)
$\nu_{i,j}$	stoichiometric coefficient (–)
α_i	$W_{cat}\cdot d_h\cdot S^{-1}\cdot C_{tot}^{-1}\cdot \mathcal{D}_i^{-1}$ ($mol^{-1}\,s\,kg$)
η^∞	effectiveness factor at $\phi\to\infty$ (–)
η	effectiveness factor (–)
δ_L	thickness of the catalytic layer (m)
ϕ	generalized Thiele modulus (–)
ε_M	macropore void fraction (–)
ε_μ	micropore void fraction (–)

References

[1] S.S. Bharadwaj, L.D. Schmidt, Fuel Process. Technol. 42 (1995) 109–127.
[2] D. Neumann, M. Kirchhoff, G. Veser, Catal. Today 98 (2004) 565–574.
[3] M. Lyubovsky, L.L. Smith, M. Castaldi, H. Karim, B. Nentwick, S. Etemad, R. LaPierre, W.C. Pfefferle, Catal. Today 83 (2003) 71–84.
[4] A.T. Ashcroft, A.K. Cheetham, J.S. Foord, M.L.H. Green, C.P. Grey, A.J. Murrel, P.D.F. Vernon, Nature 344 (1990) 319–321.
[5] P.D.F. Vernon, M.L.H. Green, A.K. Cheetham, A.T. Ashcroft, Catal. Lett. 6 (1990) 181–186.
[6] P.D.F. Vernon, M.L.H. Green, A.K. Cheetham, A.T. Ashcroft, Catal. Today 13 (1992) 417–426.
[7] S.C. Tsang, J.B. Claridge, M.L.H. Green, Catal. Today 23 (1995) 3–15.
[8] D.A. Hickman, L.D. Schmidt, J. Catal. 138 (1992) 267–282.
[9] J.B. Claridge, M.L.H. Green, S.C. Tsang, A.P.E. York, A.T. Ashcroft, P.D. Battle, Catal. Lett. 22 (1993) 299–305.
[10] D.A. Hickman, E.A. Haupfear, L.D. Schmidt, Catal. Lett. 17 (1993) 223–237.
[11] K.L. Hohn, L.D. Schmidt, Appl. Catal. A: Gen. 211 (2001) 53–68.
[12] Y.F. Chang, Heinemann, Catal. Lett. 21 (1993) 215–224.
[13] V.R. Choudary, A.M. Rajput, B. Prabhakar, J. Catal. 139 (1993) 326–328.
[14] V.R. Choudary, V.H. Rane, A.M. Rajput, Catal. Lett. 22 (1993) 289–297.
[15] V.R. Choudary, A.M. Rajput, V.H. Rane, Catal. Lett. 16 (1992) 269–272.
[16] V.R. Choudary, S.D. Sansare, A.S. Mamman, Appl. Catal. A: Gen. 90 (1992) L1–L5.
[17] Y. Boucouvalas, Z. Zhang, X.E. Verykios, Catal. Lett. 27 (1994) 131–142.
[18] T. Ioannides, X.E. Verykios, Catal. Lett. 47 (1997) 183–188.
[19] O.V. Buyevskaya, D. Wolf, M. Baerns, Catal. Lett. 29 (1994) 249–260.
[20] K. Walter, O.V. Buyevskaya, D. Wolf, M. Baerns, Catal. Lett. 29 (1994) 261–270.
[21] O.V. Buyevskaya, K. Walter, D. Wolf, M. Baerns, Catal. Lett. 38 (1996) 81–88.
[22] E.P.J. Mallens, J.H.B.J. Hoebink, G.B. Marin, J. Catal. 167 (1997) 43–56.
[23] K.H. Hofstad, J.H.B.J. Hoebink, A. Holmen, G.B. Marin, Catal. Today 40 (1998) 157–170.
[24] R. Schwiedernoch, S. Tischer, C. Correa, O. Deutschmann, Chem. Eng. Sci. 58 (2003) 633–642.
[25] D. Wang, O. Dewaele, A.M. De Groote, G.F. Froment, J. Catal. 159 (1996) 418–426.
[26] D.A. Hickman, L.D. Schmidt, AIChE J. 39 (1993) 1164–1177.
[27] A.B. Mhadeshwar, D.G. Vlachos, J. Phys. Chem. B 109 (2005) 16819–16835.
[28] J. Wei, E. Iglesia, J. Catal. 224 (2004) 370–383.
[29] J. Wei, E. Iglesia, J. Catal. 225 (2004) 116–127.
[30] G. Groppi, W. Ibashi, E. Tronconi, P. Forzatti, Chem. Eng. J. 82 (2001) 57–71.
[31] L. Majocchi, Ph.D. Thesis (1999), Politecnico di Milano.
[32] I. Tavazzi, A. Beretta, G. Groppi, P. Forzatti, in: X. Bao, Y. Xu (Eds.), Studies Surface Science Catalysis—Natural Gas Conversion VII, vol. 147, Elsevier, Amsterdam, 2004, pp. 163–168.
[33] L. Basini, M. Marchionna, A. Aragno, J. Phys. Chem. 23 (1992) 9431–9441.
[34] L. Basini, A. Aragno, J. Chem. Soc., Faraday Trans. 90 (5) (1994) 787–795.
[35] L. Basini, D. Sanfilippo, J. Catal. 157 (1995) 162–178.
[36] L. Basini, A. Aragno, G. Vlaic, Catal. Lett. 39 (1996) 49–55.
[37] T. Bruno, A. Beretta, G. Groppi, M. Roderi, P. Forzatti, Catal. Today 99 (2005) 89–98.
[38] J.G. McCarty, Catal. Today 26 (1995) 283–293.
[39] A. Beretta, P. Baiardi, D. Prina, P. Forzatti, Chem. Eng. Sci. 54 (1999) 765–773.
[40] M. Valentini, G. Groppi, C. Cristiani, M. Levi, E. Tronconi, P. Forzatti, Catal. Today 69 (2001) 307–314.
[41] W. Ibashi, G. Groppi, P. Forzatti, Catal. Today 83 (2003) 115–129.
[42] R.D. Hawthorne, After catalysts effects of heat and mass transfer between gas and catalyst surface, AIChE Symp. Ser. 70 (1974) 428–438.
[43] E. Tronconi, P. Forzatti, AIChE J. 38 (1992) 201–210.
[44] A. Beretta, G. Groppi, L. Majocchi, P. Forzatti, Appl. Catal. 187 (1999) 49–60.
[45] R.K. Shah, A.L. London, Laminar Flow Forced Convection in Ducts, Academic Press, New York, 1978.
[46] R.C. Reid, J.M. Prausnitz, B.E. Pauling, The Properties of Gases and Liquids, McGraw-Hill, New York, 1987, pp. 587–589.
[47] G.B. Froment, K.B. Bischoff, Chemical Reactor Analysis and Design, Wiley, New York, 1990.
[48] R. Burch, D.J. Crittle, M.J. Hayes, Catal. Today 47 (1999) 229–234.
[49] M. Li, J. Wei, E. Iglesia, Proceedings of the 5th World Congress on Oxidation Catalysis, Sapporo, Japan (2005) pp. 74–75.
[50] Z. Liu, P. Hu, J. Am. Chem. Soc. 125 (2003) 1958–1967.